JOURNAL OF MATERIALS SCIENCE: MATERIALS IN MEDICINE 8 (1997) 473–483

Reliability of PMMA bone cement fixation: fracture and fatigue crack-growth behaviour

N. C. NGUYEN*, W. J. MALONEY‡, R. H. DAUSKARDT*
* *Department of Materials Science and Engineering, Stanford University, Stanford, CA 94305-2205, USA*
‡ *Department of Functional Restoration, Stanford University, Stanford, CA 94305, USA*

Fracture mechanics tests were performed to characterize the fracture toughness and fatigue crack-growth behaviour of polymethylmethacrylate (PMMA) bone cement, commonly used in joint replacement surgery. Compact tension specimens of various thicknesses were prepared and tested in both air and Ringer's solution. Contrary to previous reports citing toughness as a *single valued* parameter, the PMMA was found to exhibit resistance-curve behaviour with a plateau toughness of ~ 0.6 MPa m$^{1/2}$ in air, and ~ 2.0 MPa m$^{1/2}$ in Ringer's solution. The increased toughness in Ringer's solution is thought to arise from the plasticizing effect of the environment. Under cyclic loads, the material displayed true mechanical fatigue failure in both environments; fatigue crack-growth rates, da/dN, were measured over the range $\sim 10^{-10}$ to 10^{-6} m/cycle and found to display a power-law dependence on the stress intensity range, ΔK. The cement was found to be more resistant to fatigue-crack propagation in Ringer's solution than in air. Wear debris was observed on the fatigue fracture surfaces, particularly those produced in air. These findings and the validity of using a linear-elastic fracture mechanics approach for viscoelastic materials are discussed in the context of providing more reliable and fracture-resistant cemented joints.

1. Introduction

Self-curing polymethylmethacrylate (PMMA) bone cements are extensively used to fix load-bearing prosthetic components in total joint replacement surgery. In this role, the PMMA must effectively transfer complex, time-varying physiological loads from the prosthesis to the bone [1]. Additionally, the bone cement layer provides a mechanically compliant buffer layer between the stiff metallic prosthetic substrate (elastic modulus, $E \sim 214$ GPa) and the significantly less stiff bone ($E \sim 20$ GPa) to which it is attached. Although this secondary function of the bone cement layer is often unrecognised, such functional gradation of the sandwiched layer significantly reduces localized contact stresses at the bone cement–bone interface [2] that have been implicated in progressive loosening of the joint [3]. (High interfacial contact stresses are thought to lead to a bone remodelling response involving resorption of bone at the bone–cement interface and subsequent interfacial fibrous membrane formation.)

Failure of a cemented component is most commonly associated with aseptic loosening of the joint, which may involve debonding of the metal–cement and/or cement–bone interface as well as fracture within the bone cement itself [see e.g. 4, 5, 6]. The initiating events involved with aseptic loosening are controversial and likely site dependent [5, 6]. Subsequent development of failure involving progressive debonding of the interfaces and crack growth in the bone cement are complicated by a complex biological response of the bone. The biological reactions may include interface stress and/or allergy-driven remodelling to form fibrous tissue [3, 7, 8], and reactive processes to particulate wear debris and micromotion at the interface [9, 10, 11].

While detailed consideration of these complex responses of living tissue require further elucidation if the entire loosening process is to be understood, surprisingly few studies have provided a standard measure of the fracture and subcritical crack-growth behaviour of the prosthesis–PMMA–bone structure and its individual components, particularly the PMMA bone cement. (Standard (or valid) in this context is used to indicate that fracture mechanics tests have been conducted under nominally standard conditions (e.g. as specified by ASTM E399 and E642 described in Section 4) and that results are not a function of specimen geometry and other configurational effects.) Consideration of the typical mechanical properties of the constituents of this composite structure (Table I) immediately reveals that the PMMA has significantly inferior strength and resistance to fracture. Indeed, several studies have reported that failure of femoral arthroplastic components is mediated by extensive fractures in the cement layer [4, 6, 12]. Initiation of such cracking is generally thought to begin with debonding of the bone cement from the

0957–4530

TABLE I Mechanical and elastic properties of hip implant materials

	Yield strength, σ_{ys} (MPa)	Compressive strength, σ_c (MPa)	Shear strength, σ_s (MPa)	Young's modulus, E (GPa)	Fracture toughness, K_{Ic} (MPa m$^{1/2}$)
PMMA Bone cement	24–31	66–77	30–41	2.1	0.6 (air) ~1.2 (Ringer's)
Cortical bone	133 (L) 51 (T)	193 (L) 133 (T)	68–84	15–20 (L) 11.5 (T)	2–12
Cancellous Bone	3.9	6.3	2.2	0.01–2	–
Co–Cr–Mo prosthesis	480	–	–	214	>100
Ti–6Al–4V prosthesis	940	–	–	124	90

L = longitudinal direction of loading
T = transversal direction of loading

metal prosthesis [5] and/or from voids associated with porosity either in the cement layer [13] or at the prosthesis/cement interface [14]. Under applied physiological loads, catastrophic failure of the PMMA will inevitably result in failure of the entire composite structure.

The intent of the present study is therefore to characterize both the fracture toughness and fatigue crack-growth behaviour of PMMA bone cement widely used in joint replacement surgeries. The paucity of existing fracture mechanics data can in part be attributed to the difficulty of testing very low toughness materials and to the use of non-standard specimen geometries which do not meet sample size requirements. This, in turn, leads to fracture properties that are dependent on sample size and configuration. Accordingly, a fracture mechanics approach is used to determine the plane strain fracture toughness, K_{IC}, in thick samples, and the crack-growth resistance (R-curve) behaviour in thinner samples more representative of the cement layer thickness found in joint replacements. Similarly, the fatigue crack-propagation behaviour is also examined in samples of various thicknesses. Studies were conducted in air and in simulated physiological environments, and behaviour is rationalized in terms of the prevailing deformation and fracture mechanisms.

2. Fracture mechanics background

Extensive studies have been reported on the fracture resistance of PMMA bone cements, although as noted above, few have employed standard techniques. The most widely used measure of fracture resistance, defined in linear elastic fracture mechanics (LEFM) by the plane strain fracture toughness, K_{IC}, is a single-valued material property [15]. Values in the range 0.335 to 1.6 MPa m$^{1/2}$ have been reported for PMMA [3, 12, 16, 17, 18]. Unfortunately, it is not entirely clear whether the variation described in these studies, as well as the relative ranking of different cements, can be attributed to actual material property variation (which might be associated with polymer composition, mixing and/or curing methods) or to the testing techniques employed.

Failure to meet sample size requirements may lead to fracture measurements dependent on both sample dimensions and crack size, rendering even relative rankings of fracture resistance questionable. However, using sufficiently thick fracture mechanics samples to satisfy plane strain fracture conditions may not accurately simulate the typical bone cement layer thickness of ~2 to 4 mm. The interfaces on either side of the cement layer are implicitly assumed to be weak such that they do not impose any constraint similar to that which may arise under plane strain conditions. Accordingly, Wang and Pillar [12, 19] have used a miniature short-rod fracture sample originally proposed by Barker [20] for brittle material testing, with a diameter (~4 mm) comparable to the cement layer thickness and based on an elastic–plastic analysis. These techniques, however, have a number of limitations including crack extension in a chevron-notched region (as opposed to a uniform thickness more representative of cracking configurations); artificial constructions necessary to distinguish between plasticity and crack extension effects in the interpretation of the load–displacement data; and as noted by the authors [19], an assumption of crack-size independent fracture behaviour (or flat R-curve response). However, a number of studies indicate that the micromechanisms of fracture in PMMA give rise to an energy dissipation zone surrounding the crack. This zone arises primarily from crazing ahead of the crack tip, but may on subsequent crack extension lead to crack bridging by uncracked matrix ligaments and shielding of the crack tip by the dilated crazed zone in the wake of the crack [21, 22]. These processes depend on the length of the crack, and can have a profound effect on the toughness of the material, leading to strong R-curve behaviour.

While accurate measures of the fracture toughness of PMMA are essential elements for reliable structural design, long-term structural integrity can be linked to mechanical failure from the incipient, subcritical growth of inherent material flaws or defects to critical size (defined by the fracture toughness). Cracks may be initiated from defect distributions (cracks, porosity, etc.) at either of the bimaterial interfaces (see e.g. [13, 14]) or in the bulk PMMA cement layer (see e.g.

[14, 23]). Porosity, in particular, has been linked to early crack initiation and reduced cycles to failure [14, 23]. Once initiated, subcritical crack propagation dependent on both environmental and loading conditions occurs until failure. Because the average person takes five million steps per year, cyclic fatigue crack growth is a major contributor to the failure of bone cement. Artificial hip components and fixation therefore must be designed to endure fatigue lifetimes on the order of 10^8 cycles or more.

A number of studies have addressed the fatigue endurance limit (alternating stress below which the material can endure an infinite number of cycles without failure) of bone cement [23]. However, more conservative approaches to life prediction require a detailed characterization of the fatigue crack-growth behaviour. Specifically, these analyses require relationships which define the crack-growth increment per loading cycle, da/dN, as a function of the crack-driving force, such as the applied stress intensity range, ΔK. In addition, these relationships should be obtained under representative loading and environmental conditions. Damage-tolerant lifetime predictions then entail finding the total number of loading cycles to grow an assumed or measured initial defect size to some critical size by integrating the crack-growth relationship. At present, however, there is a paucity of such subcritical crack-growth data in PMMA and very little understanding of the micromechanisms of crack growth and the synergistic effect of physiological environments.

3. Viscoelastic considerations

Most polymeric materials, including PMMA, exhibit viscoelastic constitutive behaviour. As a result, their fracture properties should ideally be characterized using viscoelastic fracture mechanics [24, 25]. Schapery [26] developed a generalized time-dependent version of the J-integral which can be used to characterize the near-tip stress and strain fields in viscoelastic materials although the complexity of the approach has precluded widespread application (see e.g. [28]). (The J-integral is an elastic–plastic fracture parameter involving a path-independent line integral around the crack tip developed assuming non-linear elastic constitutive behaviour [27]). Alternatively, a special case of generalized viscoelastic behaviour involves viscoplastic creep which can be modelled with a more simple time-dependent version of the J-integral. In such viscous materials, crack tip conditions may be uniquely defined by the C^* parameter which is the rate form of the J-integral under steady-state conditions [29, 30, 31]. In general, C^* is given by the expression [29, 30, 31, 32]

$$C^* = \int_\Gamma \left(\dot{w} \mathrm{d}y + \sigma_{ij} n_j \frac{\partial \dot{u}_j}{\partial x} \mathrm{d}s \right) \tag{1}$$

where $\dot{w}$ is the stress work rate (power) density

$$\dot{w} = \int_0^{\dot{\varepsilon}_{kl}} \sigma_{ij} \mathrm{d}\dot{\varepsilon}_{ij} \tag{2}$$

$\sigma_{ij} n_j$ are components of the traction vector, u_i are the displacement rate vector components, $\mathrm{d}s$ is a length increment along the contour Γ, and $\mathrm{d}\dot{\varepsilon}_{ij}$ is the strain rate. Recently, C^* has been used to characterize creep-crack growth in alumina [33], and to characterize the micromechanisms of creep-fatigue crack growth in silicide-matrix composites [34].

Where the extent of time-dependent viscoelastic or viscoplastic behaviour is limited, however, time-independent linear–elastic or elastic–plastic fracture mechanics may nevertheless be successfully applied to characterize fracture and fatigue crack-growth behaviour with considerably less experimental and theoretical complexity. Specifically, if the creep zone that forms ahead of a crack tip in a viscoelastic material (analogous to the plastic zone in linear–elastic fracture mechanics) is restricted in size compared to the length scales dominated by the linear–elastic $r^{-1/2}$ singularity, then small-scale creep conditions exist and LEFM can be used. Such small-scale creep conditions, however, are time dependent. At very long times, the creep zone spreads throughout the material, invalidating the use of the linear–elastic stress intensity factor, K, as the relevant characterizing parameter [35].

A key aspect in the application of LEFM is therefore to determine the transition time, t_T, from small-scale creep to extensive creep in the crack tip region. Then provided that significant crack growth occurs over time scales in comparison to the transition time, t_T, LEFM may be used. For fatigue crack growth, this condition requires that the period of the cyclically applied fatigue loads ($t_c = 1/\nu_c$, where ν_c is the cyclic loading frequency) be much smaller than t_T. However, at sufficiently high temperatures and/or low cyclic loading frequencies, the creep zone spreads throughout the entire material for $t_T \ll t_c$, and C^* becomes the appropriate characterizing parameter [35, 36, 37]. In this section, we include an analysis based on the C^* parameter to validate the use of LEFM to characterize the fracture and fatigue crack-growth behaviour of the present PMMA bone cement.

Reidel and Rice defined the characteristic time for the transition from short time to long time behaviour as [36, 37]

$$t_T = \frac{(1 - \nu^2) K^2}{(n + 1) E C^*} \tag{3}$$

where ν is Poisson's ratio, K is the maximum stress intensity factor (K_{max} of the fatigue loading cycle), E is Young's modulus, and the power-law creep relationship

$$\dot{\varepsilon} = \frac{\dot{\sigma}}{E} + A\sigma^n \tag{4}$$

determined from tensile creep data includes the creep exponent n and a material constant A.

While the experimental determination of C^* is difficult [33, 37], finite element calculations using the constitutive behaviour described by Equation 4 have shown that for the compact tension geometry used in the current study, C^* is given by the

TABLE II Creep properties and estimated values of C^* and t_T

Reference	Test mode	A (MPa^{-n} s)	n	C^* ($W\,m^{-2}$)	t_T (s)	t_T (hours)
Chwirut [39]	Compression	6.95×10^{-9}	1.7	2.2×10^{-3}	31 200	9
Norman [40]	Compression	6.9×10^{-9}	1.5	1.9×10^{-3}	38 900	11
Askeland [41]	Tension	3.6×10^{-7}	0.66	4.2×10^{-2}	1620	0.45

expression [37, 38]

$$C^* = h_1(a/W, n)\,(W - a)\,A\left[\frac{\sigma_{net}}{(1.455\eta)}\right]^{n+1} \quad (5)$$

where $h_1(a/W, n)$ is a dimensionless function of the ratio of the crack length, a, to the width of the specimen, W, $(W - a)$ is the length of the uncracked ligament ahead of the crack tip, A and n are the material constants derived from the power-law creep relationship (Equation 4), σ_{net} is the net section stress (load divided by the uncracked ligament ahead of the crack tip), and η is a dimensionless function of the crack length and the uncracked ligament.

Approximate values of C^* and associated estimates of the transition time, t_T, can now be easily obtained using creep properties of PMMA reported in the literature. Accordingly, values of the creep parameters A and n from Equation 4 were derived from published creep strain versus time data at various applied stress levels and used with Equations 5 and 3 to arrive at estimates for C^* and t_T (Table II). As very little data on tensile creep in PMMA exist, data on the compressive creep behaviour was also used to obtain values for C^* and t_T. However, because the creep properties of PMMA are not necessarily the same in tension and compression, these data should be treated with caution. Nevertheless, very similar values for the creep parameters A and n were obtained under both tension and compression in a number of studies [39, 40, 41]; these values in turn provided estimates of C^* in the range 2.0×10^{-3}–$4.2 \times 10^{-2}\ W\,m^{-2}$, corresponding to values of t_T in the range 1600–35 000 s. These estimates of the transition time from small-scale creep to large-scale creep significantly exceed the overload fracture or fatigue crack-growth cycle times contemplated in the present study. For example, in the presently reported fatigue crack-growth experiments, PMMA specimens were cycled at a frequency $\nu_c = 25$ Hz. Thus, the fatigue cycle time $t_c = 1/\nu_c = 0.04$ s, so that $t_c \ll t_T$. In addition, the loading times associated with physiological loads (walking or impact loads) are also likely to be significantly shorter than t_T. Therefore, small-scale creep conditions dominate, and the linear-elastic stress intensity factor range, ΔK, may appropriately be used as the characterizing parameter for fatigue crack-growth.

4. Experimental procedures

4.1. Material and specimen preparation

The material examined, Surgical Simplex-P radiopaque bone cement (Howmedica Inc., Rutherford, NJ), is widely available and used for total hip replacement surgery. The cement is a two-component system consisting of a powder polymer and a liquid monomer [42]. The powder polymer contains methyl methacrylate–styrene copolymer (75% w/w), polymethylmethacrylate (15% w/w), and $BaSO_4$ (10% w/w). The methacrylate–styrene copolymer provides resistance against degradation of the bone cement during gamma radiation sterilization; improves processing characteristics; and possibly reduces temperature rise during polymerization [23, 42, 43]. $BaSO_4$ imparts radiation opacity and has also been reported to improve the fracture toughness of the bone cement [23]. The liquid monomer consists of methyl methacrylate (97.4% v/v), *N*,*N*-dimethyl-paratoluidine (2.6% v/v) and 75 ± 15 p.p.m. hydroquinone.

To manufacture each specimen, 10 g of the powder polymer and 5 ml of the liquid monomer were hand-mixed at room temperature for 45 s at a rate of 1 stroke/s to reduce the formation of air bubbles. The bone cement was then transferred to a 50 mm round Delrin mould. To further reduce porosity, the mixture in the mould was capped with a Delrin plug, and then clamped to obtain a pressure of $\sim$100 kPa in the PMMA. After the specimen was allowed to cure under pressure for 30 min at room temperature, it was removed from the mould and stored in air for 24 h.

Blank samples were subsequently machined into the 50 mm diameter disc-shaped compact tension DC(T) configuration, according to the specifications of ASTM Standard E399-90 [44]. To avoid contamination, no lubricants other than water were used during the machining process. The geometry of the DC(T) specimens with width (W) of 50 mm and an initial notch length of $\sim$13 mm is shown in Fig. 1. Speci-

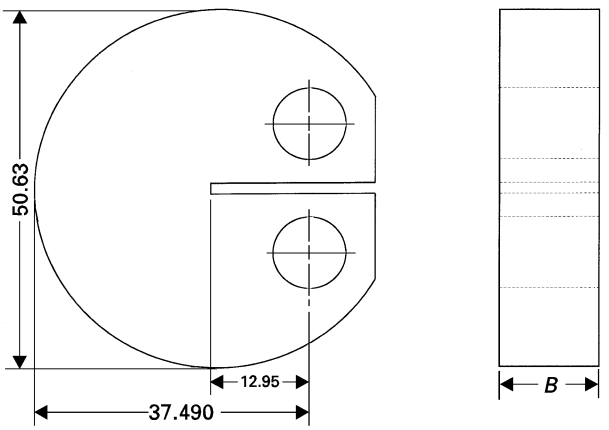

Figure 1 Geometry of the compact tension DC(T) specimen used for cyclic fatigue–crack growth and fracture toughness tests.

mens were nominally 5 mm thick (B); however, specimens of up to 15 mm thickness were also made to examine the effects of plane stress and plane strain fracture. Specimens were sanded flat and a thin (20 μm) Ni–Cr foil was bonded onto each specimen to facilitate crack length measurements described in the following section. The gauges were protected from the physiological testing environment by a thin layer of waterproof polysulphide epoxy. Salient mechanical properties of PMMA bone cement are listed in Table I.

4.2. Fatigue crack-growth

Cyclic fatigue–crack propagation rates (da/dN) were determined in general accordance with the current ASTM Standard E647-95A [45], using the procedures outlined for low toughness materials by Dauskardt and Ritchie [46] and previously applied to PMMA composites [47]. LEFM was used to characterize crack growth rates, specifically in terms of the stress intensity (K) under monotonic loading and the stress-intensity range ($\Delta K = K_{max} - K_{min}$) under cyclic loads, where K_{max} and K_{min} are the maximum and minimum values of the applied loading cycles, respectively. The stress intensity, considered the "driving force" for crack advance, provides a measure of the local stress and deformation field in the vicinity of the crack tip [15]. It is computed in terms of the applied load P and crack length a as [48, 49, 50]

$$K = \frac{P}{BW^{1/2}} f(a/w) \tag{6}$$

where $f(a/w)$ is a geometry-dependent function given for $0.3 < a/w < 1$ by [44, 48]

$$f(a/W) = \frac{[2 + (a/W)]\,[0.76 + 4.8(a/W) - 11.58(a/W)^2 + 11.43(a/W)^3 - 4.08(a/W)^4]}{[1 - (a/W)^{3/2}]} \tag{7}$$

The tests were performed using a computer-controlled, electro-servohydraulic testing system (MTS 810 load frame with 458 controller and CrackWatch fatigue-crack growth computer control system), operating under stress-intensity control. Fatigue tests were performed with a cyclic sinusoidal frequency of 25 Hz at a load ratio R (ratio of minimum to maximum loads) of 0.1 under automated load-shedding schemes to obtain growth rates over a wide range, from 10^{-10} to 10^{-6} m/cycle.

The fatigue threshold stress-intensity range, ΔK_{TH}, is the stress-intensity value below which crack growth is presumed dormant. However, as for most materials, an operational definition of ΔK_{TH} was defined as the stress-intensity range at which crack-growth rates did not exceed 10^{-10} m/cycle [45]. Under computer control, thresholds were approached by varying the applied loads such that the instantaneous values of the crack length, a, and stress intensity range, ΔK, changed according to the equation [51]

$$\Delta K = \Delta K_0 \exp[C(a - a_0)] \tag{8}$$

where a_0 and ΔK_0 are the initial values of a and ΔK, and C is the normalized K-gradient ($1/K\,dK/da$) set to ± 0.08 per mm of crack extension.

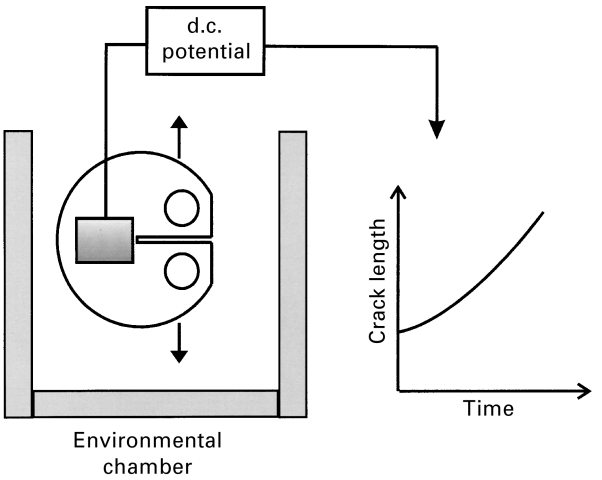

Figure 2 Schematic of the experimental method used to monitor crack length continuously using electrical potential techniques.

To initiate crack growth, a wedge-shaped starter notch was carefully cut into the specimen with a jeweller's saw. A pre-crack, approximately 3 mm long, was then grown out of this region by fatigue under displacement control. Crack propagation rates (da/dN) were continuously monitored by means of the d.c. electrical potential method [52, 53] using 20 μm thick Ni–Cr metal foils that were bonded to the specimen surfaces. The experimental set-up is schematically illustrated in Fig. 2. As the crack propagated through the specimen and metallic gauge, the changes in electrical potential across the crack (at constant current) were monitored using appropriate electronic measurement equipment. Current leakage in the electronically conducting Ringer's solution is negligible, as the electrical conductivity of the metal foil is some four to five orders of magnitude larger, and the gauge and leads were covered with a thin waterproof epoxy layer. The accuracy of the crack-length measurements relies on electrical potential calibrations for the metal foil gauge. These have been derived previously using analytical, experimental, and numerical (finite-element) techniques to a high degree of accuracy. As a result, this technique can readily detect changes in crack length of the order of $\pm$ 2 μm [52, 54]. Crack-growth rates were then determined by numerical differentiation of measurements of crack length, a, as a function of number of cycles, N. Crack-growth rate data are presented in the form of standard log–log plots of da/dN as a function of the stress intensity range, ΔK.

4.3. Fracture toughness

After completion of the fatigue tests, the fracture toughness of the PMMA was determined under displacement control from resistance curve (R-curve) behaviour. The R-curves were measured in specimens containing sharp fatigue pre-cracks at near-threshold

growth rates. Procedures essentially conform to ASTM Standard E399-90 [44], and are considered to be more precise than many used previously, where crack-length dependent fracture toughness behaviour and sample size effects were not considered. The data are presented as a graph of applied stress intensity, K_I, as a function of crack extension, Δa. Values of the fracture toughness were defined at crack initiation, K_i, and at the steady-state plateau, K_c, of the R-curve.

4.4. Environmental conditions

Baseline fracture toughness and fatigue crack-growth testing was performed in ambient temperature air at 25 °C and 45% relative humidity to facilitate comparison with other reported studies of PMMA bone cement [55, 56]. To assess the effects of a physiological environment on crack growth, tests were conducted in Ringer's solution at room temperature. The Ringer's solution was prepared with a formula of 0.66 g NaCl, 0.015 g KCl, and 0.015 g $CaCl_2$ dissolved in glass-distilled water and made up to 100 ml. The pH was monitored with a glass electrode and adjusted to 7.8 by dropwise addition of 5% $NaHCO_3$ solution. Approximately 2000 ml of this solution was used for each test, and distilled water was added periodically to the environmental chamber to replenish losses from evaporation.

5. Results

5.1. Cyclic fatigue–crack propagation

Results of the cyclic fatigue–crack growth tests at $R = 0.1$ are plotted in Fig. 3 in terms of the growth rate per cycle, da/dN, as a function of the stress intensity range, ΔK. Data were obtained at room temperature in both air and Ringer's solution. Fatigue crack-growth data has been reported for PMMA bone cement in air and is included in the figure for comparison [55, 56]. To the best of the authors' knowledge, the Ringer's solution data represent the first reported cyclic fatigue–crack propagation behaviour in a simulated physiological environment for PMMA bone cement. Crack growth rates span four orders of magnitude, from 10^{-10} to 10^{-6} m/cycle, for a range of ΔK from 0.2 to 1.6 MPa $m^{1/2}$, and show a conventional Paris power-law dependence similar to that observed in most engineering materials [57]

$$da/dN = C(\Delta K)^m \quad (9)$$

where the crack growth exponent m and the value of C are constants depending on the material and environmental couple. Average values for m and C for the air and Ringer's environment are listed in Table III. The present fatigue crack-growth data in PMMA bone cement is also compared to previous data measured in PMMA bone cement [55, 56] in Fig. 3. Although fatigue crack-growth rates measured by the previous investigators were not obtained at near-threshold values, crack-growth behaviour is clearly very similar to that observed in this investigation, with similar values of the crack-growth parameters m and C.

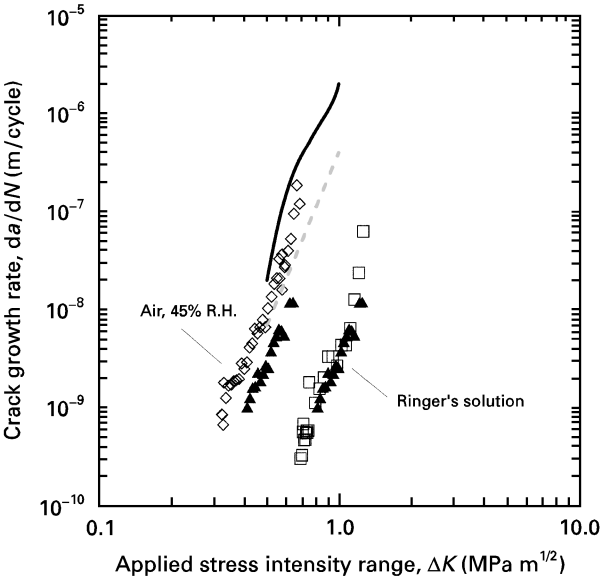

Figure 3 Experimental da/dN versus ΔK fatigue data for PMMA bone cement tested at $R = 0.10$ (25 Hz) in both air and Ringer's solution at ambient temperature. Data are compared with results for PMMA bone cement from Wright and Robinson [55] (——) and Rimnac *et al.* [56] (– – –), both tested in ambient temperature air. Sample 1 (◇) was tested in air; sample 2 (□) was tested in Ringer's solution; and sample 3 (▲) was tested in air, then in Ringer's solution.

TABLE III Paris power-law parameters and fatigue crack-growth thresholds

Environment	Fatigue threshold, ΔK_{TH} (MPa $m^{1/2}$)	Paris power-law parameters	
		Crack-growth exponent, m	C, m/cycle (MPa $m^{1/2})^{-m}$
Air	0.32	5.5	4.6×10^{-7}
Ringer's solution	0.69	5.5	3.3×10^{-9}
Air [55]	–	6.7	2.5×10^{-6}
Air [56]	–	5.8	4.0×10^{-7}

At low growth rates approaching 10^{-10} m/cycle, the bone cement is observed to display an apparent fatigue threshold stress–intensity range, ΔK_{TH}, below which crack growth is presumed dormant. The measured values of ΔK_{TH} varied between ~ 0.3–0.5 MPa $m^{1/2}$ in room temperature air, and between ~ 0.6–0.8 MPa $m^{1/2}$ in Ringer's solution. Note that while the crack-growth exponent m (slope of the fatigue crack-growth curve) is relatively unaffected by the environment, the entire fatigue crack-growth curve is shifted to higher values of ΔK when measured in Ringer's solution. The PMMA bone cement is therefore considerably more resistant to fatigue-crack propagation in Ringer's solution than in air.

5.2. Fracture toughness

Fracture toughness K_c values were determined by measuring the crack-growth R-curves of fatigue pre-cracked DC(T) samples in room temperature air and Ringer's solution. Typical R-curves for samples

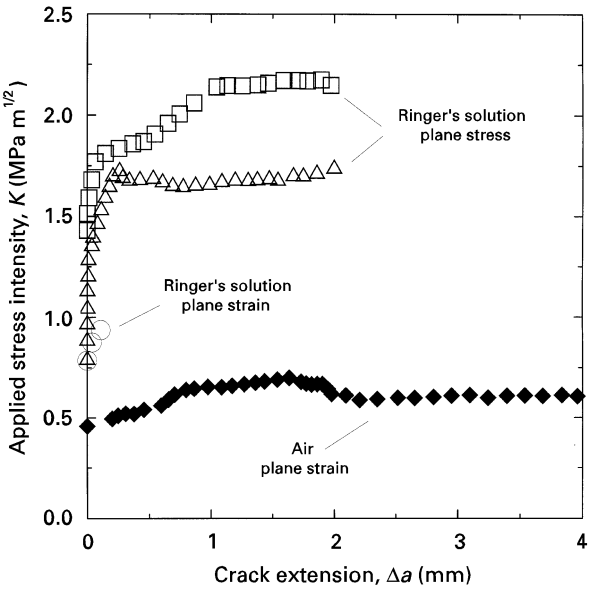

Figure 4 Resistance-curve (*R*-curve) fracture toughness behaviour for PMMA bone cement tested in Ringer's solution (open symbols) and in air (closed symbol), both at ambient temperature. (◆) Sample 1 (5 mm); (□) Sample 2 (5 mm); (△) Sample 3 (5 mm); (○) Sample 4 (15 mm).

ranging in thickness from 5 to 15 mm are illustrated in Fig. 4. Toughness values, defined at both initial crack extension (K_i) and at the steady-state plateau of the *R*-curve (K_c), are listed in Table IV. Also included in Table IV are plastic zone sizes, r_p, determined from the relation

$$r_p = \frac{1}{2\pi}\left(\frac{K_c}{\sigma_{ys}}\right)^2 \tag{11}$$

where σ_{ys} is the yield strength, and crazed zone sizes, r_c, determined from the Dugdale model for craze length [58]

$$r_c = \frac{\pi}{8}\left(\frac{K_c}{\sigma_c}\right)^2 \tag{12}$$

where σ_c is the craze yield stress, which is taken to be approximately equal to σ_{ys}.

The *R*-curves reveal that the steady-state fracture toughness of PMMA bone cement depends critically on the environment in which it is tested. In the thinner samples more representative of *in vivo* cement layer thickness, the *R*-curve plateau values were $\sim 0.6\ \text{MPa m}^{1/2}$ in air. In Ringer's solution, the *R*-curve plateau values were more than three times larger at $\sim 2.0\ \text{MPa m}^{1/2}$.

5.3. Fractography

Scanning electron micrographs of the fracture surfaces produced in PMMA bone cement during cyclic fatigue and fracture toughness testing in both air and Ringer's solution are depicted in Fig. 5. The fracture surfaces of specimens tested in air were found to be noticeably different from those tested in Ringer's solution. In addition, for each environment, fracture surfaces produced under cyclic fatigue loading differed markedly from those subjected to overload instability.

For specimens tested in air, cyclic fatigue fracture surfaces were rougher than those produced during fast fracture and also exhibited evidence of particulate wear debris. The roughest fracture surfaces were apparent at the lowest fatigue crack-growth rates (10^{-10}–10^{-8} m/cycle) (Fig. 5a). At such low crack-growth rates, the crack is able to find the easiest path through the microstructure, perhaps *around* the PMMA beads themselves. Thus, the crack follows a torturous path, and the fracture surfaces are highly irregular and uneven. Here, evidence of wear debris is most apparent. Such wear debris was presumably produced during repeated contact of asperities on mating fracture surfaces during the fatigue loading cycle. At higher fatigue crack-growth rates (10^{-7}–10^{-5} m/cycle), the fracture surfaces are progressively less rough as the crack apparently becomes less sensitive to local microstructural features (Fig. 5b). In addition, the fracture surfaces exhibit much less wear debris and begin to show signs of PMMA bead cleavage. Fracture surfaces produced by monotonic loading during fracture toughness testing were even less rough, displaying extensive evidence of PMMA bead cleavage (Fig. 5c).

Specimens tested in Ringer's solution showed nominally the same trends of decreasing fracture surface

TABLE IV *R*-curve toughness data, plastic zone sizes and crazed zone sizes

Sample	Environment	Thickness (mm)	Stress state	Fracture toughness		Plastic zones	
				K_i (MPa m$^{1/2}$)	K_c (MPa m$^{1/2}$)	$r_p^{a,b}$ (mm)	r_c^c (mm)
1	Air	5	Plane strain	0.46	0.60	0.03	0.2
2	Ringer's soln.	5	Plane stress	1.4	2.1	1.0	2.8
3	Ringer's soln.	5	Plane stress	0.80	1.7	0.7	1.8
4	Ringer's soln.	15	Plane strain	0.76	0.92	0.07	0.5

[a] For plane strain, $r_p = \frac{1}{6\pi}\left(\frac{K_c}{\sigma_{ys}}\right)^2$.

[b] For plane stress, $r_p = \frac{1}{2\pi}\left(\frac{K_c}{\sigma_{ys}}\right)^2$.

[c] For Dugdale model, $r_c = \frac{\pi}{8}\left(\frac{K_c}{\sigma_c}\right)^2$.

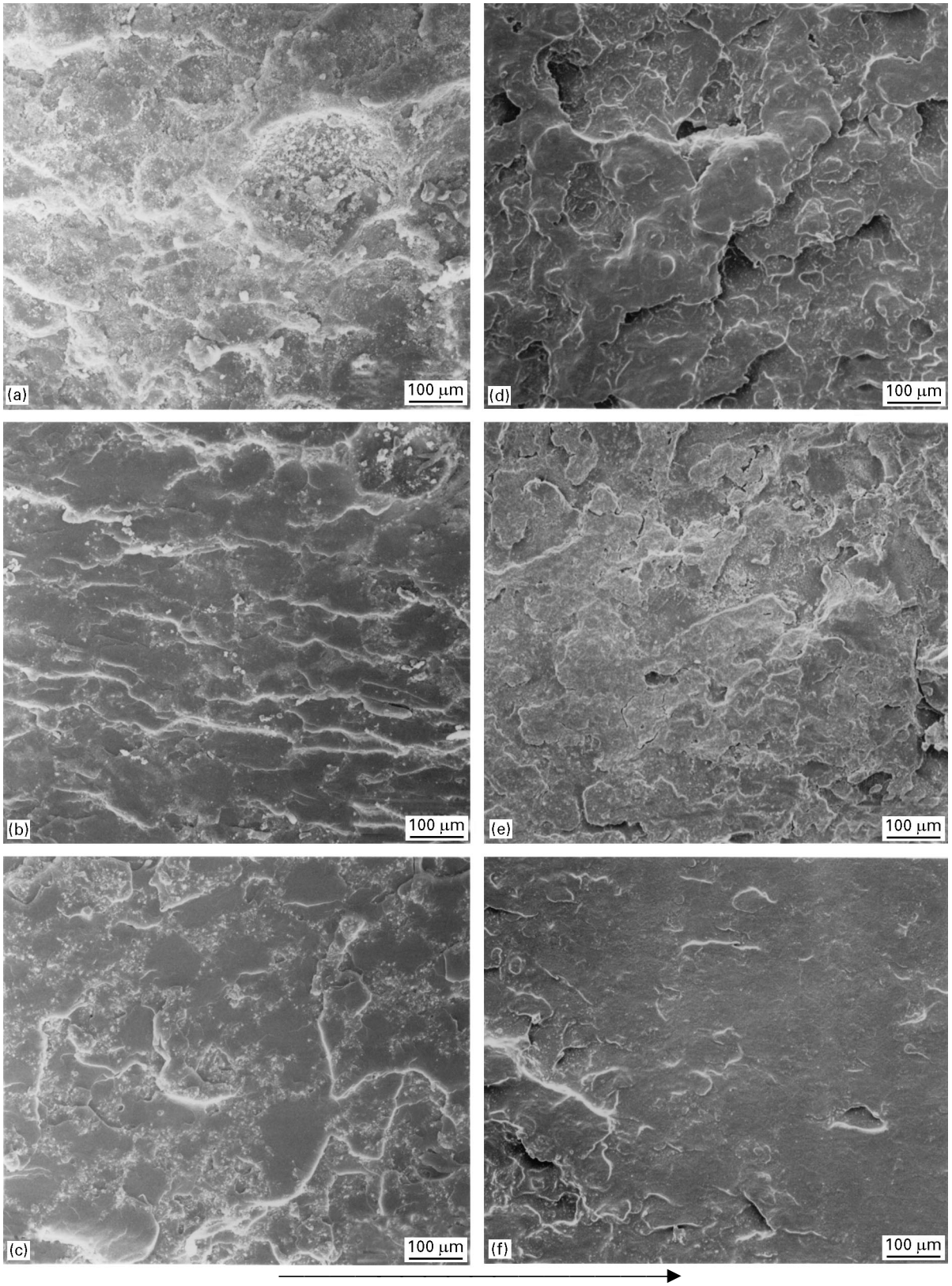

Figure 5 Scanning electron-micrographs of the fracture surfaces of PMMA tested in air (a–c) and Ringer's solution (d–f) during (a, d) cyclic fatigue-crack growth at near-threshold growth rates, (b, e) fatigue-crack growth at high growth rates, and (c, f) *R*-curve fracture toughness testing. Increasingly rough fracture surfaces are apparent after cyclic compared to monotonic loading. Also, rougher surfaces were produced in Ringer's solution compared to air. Evidence of wear debris was apparent on the fatigue surfaces produced in air. Arrow indicates general direction of crack growth.

roughness with increasing cyclic fatigue crack-growth rates and subsequent monotonic loading during fracture toughness testing. The fatigue fracture surfaces were, however, markedly more rough than the fatigue fracture surfaces produced in the air environment. Somewhat surprisingly, the increased roughness of the fatigue fracture surfaces did not lead to increased wear debris; indeed, very little evidence of wear debris was apparent (Fig. 5d, e). The aqueous environment may therefore have a lubricating effect as the fatigue fracture surfaces contact during the loading cycle.

Further surprising observations were apparent when the fast fracture surfaces produced in the air and Ringer's environments are compared (Fig. 5c and f). While the aqueous environment results in significantly rougher fracture surfaces under fatigue loading conditions, during fast fracture under monotonic loading, significantly less rough fracture surfaces were observed for samples tested in the Ringer's solution. During toughness testing in Ringer's solution, the crack cleaves cleanly through *all* of the PMMA beads in the bone cement, leaving behind a smooth, almost flat fracture surface (Fig. 5f). In contrast, during testing in air, fracture surfaces are relatively rough, and some PMMA beads remain uncleaved (Fig. 5c).

6. Discussion

The increased resistance to fatigue crack growth measured in Ringer's solution compared to that in air is thought to arise principally from the plasticizing effect of the Ringer's solution, which effectively toughens the PMMA. A similar effect of increasing toughness on shifting the entire fatigue crack-growth curve to higher values of applied ΔK (essentially decreasing fatigue crack-growth rates) has been reported for other brittle materials, including a particulate-reinforced PMMA [47], a range of transformation-toughened zirconia [46, 59], and whisker-reinforced alumina ceramics [60]. Note, however, that such effects are not consistent with fatigue crack-growth behaviour in metallic materials where growth rates are relatively insensitive to toughness [61]. An additional effect of the aqueous environment on slowing fatigue crack-growth rates may also be associated with the hydrodynamic pressures induced in the fluid as it is pumped in and out of the crack [62, 63]. These pressures act to oppose the opening or closing of the crack and therefore essentially shield the crack tip from the full applied stress intensity range.

Similar to the fatigue crack-growth behaviour, the presence of the Ringer's solution results in a plasticizing effect which enhances crazing in the crack tip region and leads to an increased fracture toughness. The presence of soluble environmental agents are well known to reduce the critical stress or strain required to initiate crazing (see e.g. [64, 65]). In addition, however, the depressed stress required to initiate crazing results in a significantly larger craze or plastic zone size ahead of the crack tip (see Table IV). As a result, the thinner samples tested in Ringer's solution do not satisfy plane strain conditions which require that the plastic zone be at least 15 times smaller than the sample thickness [44]. Similar to plane stress fracture in metals, the resulting fracture toughness displays a marked *R*-curve response with initial crack extension which may be expected to provide an additional contribution to the peak toughness achieved. In samples which were sufficiently thick to satisfy the plane-strain fracture toughness requirements (5 mm in air; 15 mm in Ringer's solution), K_c values were again $\sim 0.6\ \mathrm{MPa\,m^{1/2}}$ for samples tested in air, whereas K_c values of cement tested in Ringer's solution were almost twice as large, of the order of $1.0\ \mathrm{MPa\,m^{1/2}}$,

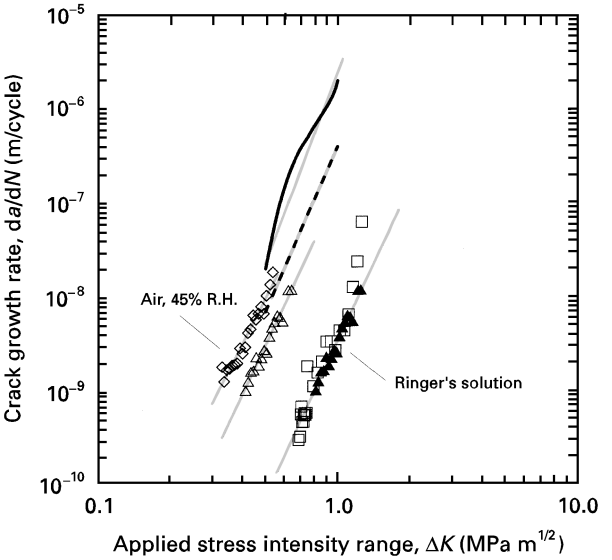

Figure 6 Best fit fatigue crack-growth relationships typically used for life prediction methodologies shown in comparison to the experimental da/dN versus ΔK data. Data are compared with results for PMMA bone cement from Wright and Robinson [55] (——) and Rimnac *et al.* [56] (– – –), both tested in ambient temperature air. (◇) Sample 1: $C = 4.7 \times 10^{-7}$, $m = 5.5$; (□) Sample 2: $C = 3.3 \times 10^{-9}$, $m = 5.5$; (▲) Sample 3; $C = 3.3 \times 10^{-9}$, $m = 5.5$; (△) Sample 3: $C = 1.3 \times 10^{-7}$, $m = 5.4$. Shaded lines are best fit to data.

but less than the three-fold increase measured in the thinner plane-stress samples.

In general, fatigue crack-growth rates for PMMA appear to display a much higher sensitivity to the applied ΔK range than typically observed for metallic materials, as evidenced by the steeper slopes and higher crack growth exponents *m*. The worst-case data for the PMMA bone cement tested in air can be represented by the crack-growth rate relationship

$$da/dN = 4.6 \times 10^{-7}(\Delta K)^{5.5} \qquad (10)$$

Best fit crack-growth relationships for the current fatigue crack-growth data are shown in Fig. 6. Fracture mechanics based damage-tolerant design procedures which are intended to provide a conservative (worst-case) estimate of the structural life in terms of the time (or stress cycles) for the largest undetected crack to grow to critical size typically rely on such characterization of the fatigue crack-growth rate [57, 66]. The majority of such data are typically derived from through-thickness, *long* cracks (typically ~2 to 20 mm in length) growing in conventional fracture mechanics specimens. It should be pointed out, however, that such cracking configurations rarely simulate reality for *in service* failures of prostheses, which generally occur in the small component cross-sections by subcritical crack growth from smaller, pre-existing flaws. A more complete analysis must therefore include the apparently rapid growth of small cracks. This is particularly important since it is well known for metal fatigue [67], and has recently become apparent for the fatigue of ceramics [59, 60], that where cracks are physically small (typically less than ~500 μm in size), or small compared to microstructural dimensions or the extent of local crack-tip inelasticity, their growth rates can be far in excess of

corresponding long cracks subjected to the same applied K levels; moreover, small cracks are known to propagate at stress intensities less than the fatigue threshold, below which long cracks are presumed dormant [59, 60, 67].

7. Conclusions

Based on a study of cyclic fatigue–crack growth and fracture behaviour of PMMA bone cement, a polymeric material used to affix load-bearing prostheses to bone in joint replacement surgery, the following conclusions can be made:

1. Physiological environment has a profound effect upon both cyclic fatigue crack-growth and fracture toughness behaviour of PMMA bone cement. Specifically, the PMMA is more resistant to both cyclic fatigue and fracture in Ringer's solution (a simulated physiological environment) than in 45% relative humidity laboratory air.
2. Cyclic-fatigue crack growth rates, da/dN, in PMMA bone cement exhibited a conventional Paris power-law dependence on the linear–elastic stress-intensity range, ΔK. Fatigue threshold values (ΔK_{TH}), operationally defined at growth rates below $\sim 10^{-9}$ m/cycle, were observed to be in the range ~ 0.3–$0.5\ \mathrm{MPa\,m^{1/2}}$ in air and ~ 0.6–$0.8\ \mathrm{MPa\,m^{1/2}}$ in Ringer's solution.
3. In samples thick enough to satisfy the small-scale yielding requirements for fracture toughness, K_c values for PMMA bone cement were $\sim 0.6\ \mathrm{MPa\,m^{1/2}}$ in air and $\sim 1.0\ \mathrm{MPa\,m^{1/2}}$ in Ringer's solution. In thinner samples more representative of *in vivo* cement layer thickness, R-curve plateau values were $\sim 0.6\ \mathrm{MPa\,m^{1/2}}$ in air and in the range ~ 1.75–$2.25\ \mathrm{MPa\,m^{1/2}}$ in Ringer's solution. Thinner samples tested in Ringer's solution exhibited pronounced R-curve toughness behaviour.
4. Fracture surfaces of specimens tested in air differ markedly from those specimens tested in Ringer's solution. The roughness of samples generally decreased with increasing fatigue growth rates and were the least rough under monotonic loading. Fatigue fracture surfaces were significantly more rough when produced in the simulated physiological environment, although the fast fracture surfaces were significantly less rough.
5. Wear debris was apparent on the fatigue fracture surfaces, particularly those produced in the air environment. Wear debris is thought to arise from wear processes during repeated contact of asperities on mating fracture surfaces during the fatigue loading cycle. Surprisingly, while the significantly rougher fracture surfaces produced during fatigue crack growth in the physiological environment might be thought to produce more wear debris, less debris was actually observed. This is presumably due to both the lubricating effect of the aqueous environment and its effect on increasing ductility in the polymer. Such fracture processes are considered important as they elucidate the *in vivo* failure mechanisms and generation of wear debris in PMMA.
6. Characterization and understanding of fracture and cyclic fatigue crack-growth behaviour of PMMA bone cement will lead to more reliable structural design of prosthetic joints. In addition, this knowledge will provide the basis for more accurate life predictions and improvement of the structural integrity of cemented load-bearing prostheses.

Acknowledgements

The authors would like to thank Dr Lane Smith of the Department of Functional Restoration, Stanford University for useful discussions. The Surgical Simplex-P bone cement was kindly supplied by Dr Ray Leskanic of Howmedica Inc., Rutherford, NJ. The work was funded by a Dana Adams Griffin Award received by R. H. D. from the McCutchen Foundation.

References

1. J. CHARNLEY, in "Acrylic cement in orthopedic surgery" (Williams and Wilkins, Baltimore, 1970).
2. F. ERDOGAN and G. D. GUPTA, *J. Appl. Mech.* **38** (1971) 937.
3. A. S. LITSKY and R. M. ROSE, *J. Ortho. Res.* **8** (1990) 623.
4. U. E. PAZZAGLIA, *Arch. Ortho. Traum. Surg.* **109** (1990) 83.
5. M. JASTY, W. J. MALONEY, C. R. BRAGDON, D. O. O'CONNOR, T. HAIRE and W. H. HARRIS, *J. Bone Joint Surg.* (*Br*) **73-B** (1991) 551.
6. E. J. CHEAL, M. SPECTOR and W. C. HAYES, *J. Ortho. Res.* **10** (1992) 405.
7. B. MJOBERG, *Acta Ortho. Scan.* **57** (Suppl) (1986) 5.
8. E. M. EVANS, M. A. R. FREEMAN, A. J. MILLER and B. VERNON-ROBERTS, *J. Bone Joint Surg.* (*Br*) **56** (1974) 626.
9. P. A. REVELL, B. WEIGHTMAN, M. A. R. FREEMAN and B. VERNON-ROBERTS, *Arch. Ortho. Traum. Surg.* **81** (1978) 167.
10. S. R. GOLDRING, M. JASTY, M. ROELKE, K. K. PETRISON, F. R. BRINGHURST, A. L. SCHILLER and W. H. HARRIS, in Non-Cemented Total Hip Arthroplasty, Proceedings of the 3rd Annual Bristol-Myers/Zimmer Orthopaedic Symposium, Phoenix, March 1987, edited by R. H. Fitzgerald, Jr. (Raven Press, New York, 1988) p. 35.
11. S. B. GOODMAN, "The effects of micromotion and particulate materials on tissue differentiation, "*Acta Ortho. Scan.* **65** (Suppl. 258) (1994) 1.
12. C. T. WANG and R. M. PILLIAR, *J. Mater. Sci.* **24** (1989) 3725.
13. V. M. GHARPURAY, L. M. KEER and J. L. LEWIS, *J. Biomech. Eng.* **112** (1990) 22.
14. S. P. JAMES, T. P. SCHMALZRIED, F. J. MCGARRY and W. H. HARRIS, *J. Biomed. Mater. Res.* **27** (1993) 71.
15. G. R. IRWIN, in "Handbuch der Physik VI", Vol. 6, edited by S. Flugge (Springer, Berlin, 1958) p. 558.
16. L. D. T. TOPOLESKI, P. DUCHEYNE and J. M. CUCKLER, *J. Biomed. Mater. Res.* **26** (1992) 1617.
17. B. POURDEYHIMI, H. D. WAGNER and P. SCHWARTZ, *J. Mater. Sci.* **21** (1986) 4468.
18. J. L. HAILEY, I. G. TURNER and A. W. MILES, *Adv. Biomater.* **10** (1992) 325.
19. C. T. WANG and R. M. PILLIAR *J. Mater. Sci.* **24** (1989) 2391.
20. L. M. BARKER, *Eng. Fract. Mech.* **9** (1977) 361.
21. R. W. HERTZBERG, in "Deformation and fracture mechanics of engineering materials" (John Wiley & Sons, Inc., New York, 1989) p. 388.
22. A. G. ATKINS and Y.-W. MAI, in "Elastic and plastic fracture" (Ellis Horwood Limited, Chichester, 1985) p. 44, 401.
23. S. SAHA, in Proceedings of the Eighth Annual Conference of the IEEE/Engineering in Medicine and Biology Society, Fort

Worth, November 1986, edited by G. V. Kondraske and C. J. Robinson (IEEE, New York, 1986) p. 1672.
24. T. L. ANDERSON, in "Fracture mechanics: fundamentals and applications" (CRC Press, Inc., Boca Raton, 1991) p. 131.
25. T. H. COURTNEY, in "Mechanical behaviour of materials" (McGraw-Hill Publishing Company, New York, 1990) p. 65.
26. R. A. SCHAPERY, in Encyclopedia of Materials Science and Engineering, edited by Robert Cahn (Pergamon Press, Oxford, 1986) p. 5043.
27. J. R. RICE, *J. Appl. Mech.* **35** (1968) 379.
28. C. D. BENCHER, R. H. DAUSKARDT and R. O. RITCHIE, *J. Spacecraft Rockets* **32** (1995) 328.
29. J. D. LANDES and J. A. BEGLEY, in Proceedings of the Eighth National Symposium on Fracture Mechanics, Providence, August 1974, edited by J. R. Rice and P. C. Paris, (American Society for Testing and Materials, Philadelphia, 1976) p. 128.
30. K. OHJI, K. OGURA, and S. KUBO, *Trans. Japan. Soc. Mech. Eng.* **42** (1976) 350.
31. K. M. NIKBIN, G. A. WEBSTER and C. E. TURNER, in Proceedings of the Ninth National Symposium on Fracture Mechanics, Pittsburgh, August 1975, edited by J. L. Swedlow and M. L. Williams (American Society for Testing and Materials, Philadelphia, 1976) p. 47.
32. T. L. ANDERSON, in "Fracture mechanics: fundamentals and applications" (CRC Press, Inc., Boca Raton, 1991) p. 256.
33. G. MARTIN, T. FETT and D. MUNZ, *J. Eur. Ceram. Soc.* **15** (1995) 643.
34. U. RAMAMURTY, A. S. KIM, S. SURESH and J. J. PETROVIC, *J. Amer. Ceram. Soc.* **76** (1993) 1953.
35. T. L. ANDERSON, in "Fracture mechanics: fundamentals and applications" (CRC Press, Inc., Boca Raton, 1991) p. 259.
36. H. RIEDEL and J. R. RICE, in Proceedings of the Twelfth National Symposium on Fracture Mechanics, edited by P. C. Paris (American Society for Testing and Materials, Philadelphia, 1980) p. 112.
37. H. RIEDEL, in "Fracture at high temperatures" (Springer-Verlag, Berlin, 1987) p. 308.
38. V. KUMAR, M. D. GERMAN and C. F. SHIH, in "An engineering approach for elastic–plastic fracture analysis," EPRI NP-1931 (Electric Power Research Institute, Palo Alto, CA, 1981) p. 3.
39. D. J. CHWIRUT, *J. Biomed. Mater. Res.* **18** (1984) 25.
40. T. L. NORMAN, V. KISH, K. HUSTOSKY, and J. D. BLAHA, in "Advances in bioengineering", edited by J. M. Tarbell American Society of Mechanical Engineers, **26** (1993) 247.
41. D. R. ASKELAND, in "The Science and Engineering of Materials" (PWS Publishing Company, Boston, 1994) p. 490.
42. M. JASTY, J. P. DAVIES, D. O. O'CONNOR, D. W. BURKE, T. P. HARRIGAN and W. H. HARRIS, *Clin. Orthop.* **259** (1990) 122.
43. S. S. HAAS, G. M. BRAUER and G. D. DICKSON, *J. Bone Joint Surg.* **57-A** (1975) 380.
44. ASTM Standard E399-90, in "1994 ASTM Annual Book of Standards," Vol. 3.01 (American Society for Testing and Materials, Philadelphia, 1994) p. 673.
45. ASTM Standard E647-95, in "1995 ASTM Annual Book of Standards," Vol. 3.01 (American Society for Testing and Materials, Philadelphia, 1995) p. 578.
46. R. H. DAUSKARDT and R. O. RITCHIE, *Closed Loop* **17** (1989) 7.
47. C. SHEU, R. H. DAUSKARDT and L. DE JONGHE, *J. Mater. Sci.* **28** (1993) 2196.
48. H. TADA, P. C. PARIS and G. R. IRWIN, in "Stress analysis of cracks handbook" (Paris Productions, Inc./Del Research Corp., St. Louis, 1985).
49. J. C. NEWMAN, in Proceedings of the Seventh National Symposium on Fracture Mechanics, College Park, August 1973, edited by P. C. Paris and G. R. Irwin (American Society for Testing and Materials, Philadelphia, 1974) p. 105.
50. J. E. SRAWLEY, *Int. J. Fract.* **12** (1976) 475.
51. A. SAXENA, S. J. HUDAK, J. K. DONALD and D. W. SCHMIDT, *J. Test. Eval.* **6** (1978) 167.
52. G. H. ARONSON and R. O. RITCHIE, *ibid.* **7** (1979) 208.
53. D. A. UTAH, W. H. CULLEN, R. O. RITCHIE, R. H. STENTZ and R. WILLIAMS, in "Metals handbook, 9th edition, Volume 8, Mechanical Testing", edited by J. R. Newby, J. R. Davis and S. K. Refsnes (American Society for Metals, Metals Park, OH, 1985) p. 376.
54. P. K. LIAW, H. R. HARTMANN and W. A. LOGSDON, *J. Test. Eval.* **11** (1983) 202.
55. T. M. WRIGHT and R. P. ROBINSON, *J. Mater. Sci.* **17** (1982) 2463.
56. C. M. RIMNAC, T. M. WRIGHT and D. L. MCGILL, *J. Bone Joint Surg.* **68-A** (1986) 281.
57. R. W. HERTZBERG, in "Deformation and fracture mechanics of engineering materials" (John Wiley & Sons, Inc., New York, 1989) p. 579.
58. A. G. ATKINS and Y.-W. MAI, in "Elastic and plastic fracture" (Ellis Horwood Limited, Chichester, 1985) p. 408.
59. R. H. DAUSKARDT, D. B. MARSHALL and R. O. RITCHIE, *J. Amer, Ceram. Soc.* **73** (1990) 893.
60. R. H. DAUSKARDT, M. R. JAMES, J. R. PORTER and R. O. RITCHIE, *ibid.* **75** (1992) 759.
61. R. O. RITCHIE, *Int. Met. Rev.* **20** (1979) 205.
62. J. L. TZOU, C. H. HSUEH, A. G. EVANS and R. O. RITCHIE, *Acta. Metall.* **33** (1985) 117.
63. K. S. YI, S. J. DILL and R. H. DAUSKARDT, *ibid.* **44** (1996) in review.
64. R. P. KAMBOUR, C. L. GRUNER and E. E. ROMAGOSA, *Macromolecules* **7** (1974) 248.
65. N. BROWN, in "Methods of experimental physics", Vol. 16, Part C, edited by R. A. Fava (Academic Press, New York, 1980) p. 233.
66. R. H. DAUSKARDT, R. O. RITCHIE, J. K. TAKEMOTO and A. M. BRENDZEL, *J. Biomed. Mater. Res.* **28** (1994) 791.
67. R. O. RITCHIE and J. LANKFORD (eds), "Small fatigue cracks" (The Metallurgical Society of AIME, Warrendale, PA, 1986) p. 665.

Received 13 May 1996
and accepted 13 February 1997